Optically Functional Di-Urethanesil Nanohybrids Containing Eu^{3+} Ions

M. C. Gonçalves,[†] V. de Zea Bermudez,*[,†] R. A. Sá Ferreira,[‡] L. D. Carlos,*[,‡] D. Ostrovskii,[||] and J. Rocha[§]

Departamento de Química and CQ-VR, Universidade de Trás-os-Montes e Alto Douro and CQ-VR, Quinta de Prados, Apartado 1013, 5000-911 Vila Real, Portugal, Departamento de Física and CICECO, and Departamento de Química and CICECO, Universidade de Aveiro, 3810-193 Aveiro, Portugal, and Department of Applied Physics, Chalmers University of Technology, 41296 Göteborg, Sweden

Received September 19, 2003. Revised Manuscript Received April 20, 2004

Sol−gel derived poly(oxyethylene)/siloxane hybrids (di-urethanesils) doped with europium triflate, $Eu(CF_3SO_3)_3$, were examined by XRD, ^{13}C and ^{29}Si MAS NMR and FT-IR, FT-Raman, and photoluminescence spectroscopies. The host framework of these materials consists of a siliceous network grafted through urethane linkages to both ends of polymer chains with 6 oxyethylene repeat units. Xerogels with $\infty \geq n \geq 1$ (where n is the molar ratio $(OCH_2CH_2)/Eu^{3+}$) were analyzed. The compounds with $n \geq 10$ are amorphous. In samples with $n \leq 5$ crystalline $Eu(CF_3SO_3)_3$ was detected. In the di-urethanesils with $n \geq 10$ the cations interact with the urethane carbonyl oxygen atoms. The complexation of the polyether chains to the cations is initiated at approximately $n = 10$. At $n \leq 10$ both types of cation bonding situations occur. "Free" and weakly coordinated $CF_3SO_3^-$ ions exist in the whole range of salt concentrations analyzed. Ionic aggregates are formed in samples with $n = 5$ and 1. For $200 \geq n \geq 20$ the emission quantum yields range from 0.7 to 8.1%. The decrease in the quantum yield with the increase of the Eu^{3+} concentration markedly depends on the activation of the energy transfer between the hybrid host's emitting centers and the cations, permitting, therefore, a fine-tuning of the emission chromaticity across the CIE (Commission Internationale d'Éclairage) diagram (e.g., (x, y) color coordinates from (0.19, 0.18) to (0.50, 0.49), for $n = 200$ and 5, respectively).

I. Introduction

Sol−gel chemistry is considered an excellent approach for the preparation of advanced tailor-made nanohybrid materials with extraordinary technological impact in a wide variety of applications.[1−13] The potential advantages of the sol−gel route with respect to other classical synthetic procedures include relatively low-temperature processing, higher purity, improvement of the thermal and dimensional stability of the resulting compounds, and easy shaping into thin films, fibers, and monoliths. The possibility of combining the organic and inorganic components at the nanosize level is another advantage offered by the sol−gel method which has opened challenging new prospects in the area of nanohybrid materials.

With the goal of developing materials with high quantum efficiency for application in optics, sol−gel derived poly(oxyethylene) (POE)/siloxane frameworks were employed. These hybrid structures are of the utmost interest, not only in the context of optics, but also for the fabrication of multifunctional single-material-based devices.[14−18] The di-urea cross-linked POE/siloxane hybrids (di-ureasils)[19] doped with Eu^{3+} ions are

* Authors to whom correspondence should be addressed. Tel: 351-259-350253. Fax: 351-259-350480. E-mail: vbermude@utad.pt. Tel: 351-234-370946. Fax: 351-234-424965. E-mail: lcarlos@fis.ua.pt.

[†] Universidade de Trás-os-Montes e Alto Douro.

[‡] Departamento de Física and CICECO, Universidade de Aveiro.

[§] Departamento de Química and CICECO, Universidade de Aveiro.

[||] Chalmers University of Technology.

(1) Brinker, C. J.; Scherer, G. W. *Sol−Gel Science, The Physics and Chemistry of Sol−Gel Processing*; Academic Press: San Diego, CA, 1990.

(2) (a) Schubert, U.; Hüsing, N.; Lorenz, A. *Chem. Mater.* **1995**, *7*, 2010. (b) Sanchez, C.; Ribot, F.; Lebeau, B. *J. Mater. Chem.* **1999**, *9*, 35. (c) Stupp, S. I.; Braun, P. V. *Science* **1999**, *277*, 1242.

(3) (a) *Better Ceramics Through Chemistry VII: Organic/Inorganic Hybrid Materials*; Coltrain, B. K., Sanchez, C., Schaefer, D. W., Wilkes, G. L., Eds.; Materials Research Society Series Vol. 435; MRS: Pittsburgh, PA, 1996. (b) *Organic/Inorganic Hybrid Materials-2000*; Laine, R., Sanchez, C., Brinker, C. J., Gianellis, E., Eds.; Materials Research Society Series Vol. 628; MRS: Pittsburgh, PA, 2000.

(4) *Sol−Gel Optics V*; Dunn, B. S., Pope, E. J. A., Schmidt, H. K., Yamane, M., Eds.; SPIE Series Vol. 3943; The International Society of Optical Engineering: Bellingham, WA, 2000.

(5) Stein, A.; Melde, B. J.; Schroden, R. C. *Adv. Mater.* **2000**, *12*, 1403.

(6) Chujo, Y.; Tamaki, R. In *Hybrid Organic−Inorganic Materials*; Loy, D. A., Ed.; *Mater. Res. Soc. Bull.* **2001**, *26*, 389.

(7) Sanchez, C.; Soler-Illia, G. J. de A. A.; Ribot, F.; Lalot, T.; Mayer, C. R.; Cabuil, V. *Chem. Mater.* **2001**, *13*, 3061.

(8) Keeling-Tucker, T.; Brennan, J. D. Special issue on *Hybrid Organic−Inorganic Materials; Chem. Mater.* **2001**, *13*, 3331.

(9) Green, W. H.; Le, K. P.; Grey, J.; Au, T. T.; Sailor, M. J. *Science* **1997**, *276*, 1826.

(10) Lin, J.; Baerner, K. *Mater. Lett.* **2000**, *46*, 86.

(11) Arkles, B. In *Hybrid Organic−Inorganic Materials*,; Loy, D. A., Ed.; *Mater. Res. Soc. Bull.* **2001**, *26*, 402.

(12) Schottner, G. *Chem. Mater.* **2001**, *13*, 3422.

(13) Jeong Cho, E.; Bright; F. V. *Anal. Chem.* **2002**, *74*, 1462.

(14) (a) Amaral, V.; Carlos, L. D.; De Zea Bermudez, V. *IEEE Trans. Magn.* **2001**, *37*, 2935.

10.1021/cm0348848 CCC: $27.50
Published on Web 06/02/2004

extremely attractive because they behave as white-light intrinsic phosphors and their color can be readily tuned through the variation of the excitation wavelength.[16b−18] (The di-ureasils are composed of short POE chains of variable length covalently bonded at both ends to a siliceous network through urea groups (−NHC(=O)-NH−). These matrixes were designated as d-U(*Y*), where d represents di, U indicates the urea group, and *Y* denotes the average molecular weight of the diamine precursor used (Y = 2000, 900, and 600 g·mol^{-1}, corresponding to about 41, 16, and 9 (OCH_2CH_2) repeat units, respectively)).

The di-urethane cross-linked POE/siloxane networks (di-urethanesils)[20] are another interesting family of hybrids. (The di-urethanesils are composed of a siliceous network grafted through urethane (−NH(C=O)O−) groups to both ends of poly(ethylene glycol) (PEG) segments. These matrixes were represented by d-Ut-(*Y*′), where Ut denotes urethane and *Y*′ indicates the average molecular weight of the starting PEG molecule (Y' = 2000, 600, and 300 g·mol^{-1}, corresponding to approximately 45, 13, and 6 (OCH_2CH_2) repeat units, respectively).) A thorough study devoted to the calculation of the RT photoluminescent external quantum yields of the nondoped di-ureasil and di-urethanesil hybrids provided conclusive evidence that the values obtained depended on the nature of the cross-linkages and, in the case of the urethane cross-linked networks, also on the polymer chain length.[21] The quantum yield found for d-Ut(2000) is similar to the value measured for 3-aminopropyltriethoxysilane (APTES) with carboxyl acids (0.35 ± 0.1), which are the most efficient intrinsic phosphors reported to date.[9] This evidence prompted us to focus our attention on the Eu^{3+}-doped di-urethanesil system, for which higher quantum yields than those found in the urea cross-linked analogues[16g] may, in principle, be expected.

A preliminary infrared and Raman spectroscopic analysis of d-Ut(300)$_n$Eu(CF_3SO_3)$_3$ xerogels with $\infty \geq n \geq 5$ (where *n*, so-called composition, represents the number of ether oxygen atoms per Eu^{3+} ion) was performed with the goal of assessing the local environment around the lanthanide ions as a function of salt concentration.[20a] The study of the structure of the d-Ut-(300)$_n$Eu(CF_3SO_3)$_3$ nanocomposites was initiated recently using small angle X-ray scattering.[20b]

In the present work we continue the investigation of the family of the Eu^{3+}-doped d-Ut(300)-based di-urethanesils through the analysis of a set of samples with a wider range of Eu(CF_3SO_3)$_3$ concentration ($n \geq 1$). Their morphology and structure will be examined by means of solid state ^{29}Si and ^{13}C magic angle spinning (MAS) nuclear magnetic resonance (NMR) and X-ray diffraction (XRD). Photoluminescence emission (PL) and excitation (PLE) spectroscopy, Fourier transform infrared (FT-IR), and Fourier transform Raman (FT-Raman) spectroscopies will be employed to gain insight into both the cationic and anionic environments in the di-urethanesils. PL will be also used to determine the chromaticity coordinates of the d-Ut(300)$_n$Eu(CF_3SO_3)$_3$ system, to calculate the absolute external quantum yields of representative materials, and to discuss the activation/deactivation of host-to-metal energy transfer mechanisms.

II. Experimental Section

Materials. Europium(III) trifluoromethanesulfonate, or triflate, (Eu(CF_3SO_3)$_3$, Aldrich) and 3-isocyanatepropyltriethoxysilane (ICPTES, Fluka) were used as received. Poly(ethylene glycol) (PEG, Aldrich, $M_w \approx 300$ g·mol^{-1}), tetrahydrofuran (THF, Merck), and ethanol (CH_3CH_2OH, Merck) were stored over molecular sieves. High-purity distilled water was used in all experiments.

Synthesis. The first stage of the synthesis of the di-urethanesils involved the formation of covalent urethane linkages between the terminal hydroxyl groups of a poly(ethylene glycol) including about 6 oxyethylene units, PEG(300), and the isocyanate groups of the alkoxysilane precursor ICPTES. In the second stage of the synthesis water and ethanol were added to promote the hydrolysis and condensation reactions characteristic of the sol−gel process. The guest lanthanide salt was added in the latter step. Xerogel materials with *n* between ∞ and 1 were prepared.

Step 1. Synthesis of the di-Urethanesil Hybrid Precursor, d-UtPTES(300) (Scheme 1). A 1.5-g portion of PEG(300) was dissolved in 10 mL of THF by stirring. A volume of 2.469 mL of ICPTES was added to this solution in a fume cupboard (molar proportion 2:1 ICPTES/PEG(300)). The flask was then sealed and the solution was stirred for 24 h at moderate temperature (approximately 70 °C). The grafting process was infrared monitored. During the formation of the urethane cross-links the intensity of the prominent and sharp absorption band located at 2273 cm^{-1}, ascribed to the stretching vibration of the isocyanate group of the ≡Si−$(CH_2)_3$−N=C=O moiety, progressively decreased, until it disappeared upon completion of the reaction. These spectral changes were accompanied by the growth of a series of new bands produced by the urethane group in the 1760−1530 cm^{-1} spectral region. The d-UtPTES(300) compound was obtained as a transparent oil. ^{1}H NMR ($CDCl_3$, 400.13 MHz) δ (ppm) 5.02 (sb, 2H, H^g), 3.79 (m, 12 H,

(15) (a) de Zea Bermudez, V.; Carlos, L. D.; Duarte, M. C.; Silva, M. M.; Silva, C. J.; Smith, M. J.; Assunção, M.; Alcácer, L. *J. Alloys Compd.* **1998**, *275*−*277*, 21. (b) Silva, M. M.; de Zea Bermudez, V.; Carlos, L. D.; Passos de Almeida, A. P.; Smith, M. J. *J. Mater. Chem.* **1999**, *9*, 1735. (c) Silva, M. M.; de Zea Bermudez, V.; Carlos, L. D.; Smith, M. J. *Electrochim. Acta* **2000**, *45*, 1467. (d) Gomes Correia, S. M.; de Zea Bermudez, V.; Silva, M. M.; Barros, S.; Sá Ferreira, R. A.; Carlos, L. D.; Smith, M. J. *Ionics* **2002**, *8* (1&2), 73. (e) Gomes Correia, S. M.; de Zea Bermudez, V.; Silva, M. M.; Barros, S.; Sá Ferreira, R. A.; Carlos, L. D.; Smith, M. J. *Electrochim. Acta* **2002**, *47*, 2551. (f) Silva, M. M.; de Zea Bermudez, V.; Carlos, L. D.; Smith, M. J. *Ionics* **1998**, *4*, 170.

(16) (a) Carlos, L. D.; de Zea Bermudez, V.; Sá Ferreira, R. A. *J. Non. Cryst. Solids* **1999**, *247*, 203. (b) Carlos, L. D.; Sá Ferreira, R. A.; de Zea Bermudez, V.; Molina, C.; Bueno, L. A.; Ribeiro, S. J. L. *Phys. Rev. B* **1999**, *60*, 10042. (c) Carlos, L. D.; Messaddeq, Y.; Brito, H. F.; Sá Ferreira, R. A.; de Zea Bermudez, V.; Ribeiro, S. J. L. *Adv. Mater.* **2000**, *12*, 594. (d) Carlos, L. D.; Sá Ferreira, R. A.; de Zea Bermudez, V. *Electrochim. Acta* **2000**, *45*, 1467. (e) Molina, C.; Ribeiro, S. J. L.; Dahmouche, K.; Santilli, C. V.; Craievich, A. F. *J. Sol-Gel Sci. Technol.* **2000**, *19*, 615. (f) de Zea Bermudez, V.; Sá Ferreira, R. A.; Carlos, L. D.; Molina, C.; Dahmouche, K.; Ribeiro, S. J. L. *J. Phys. Chem. B* **2001**, *105*, 3378. (g) Sá Ferreira, R. A.; Carlos, L. D.; Gonçalves, R. R.; Ribeiro, S. J. L.; de Zea Bermudez, V. *Chem. Mater.* **2001**, *13*, 2991. (h) Dahmouche, K.; Carlos, L. D.; de Zea Bermudez, V.; Sá Ferreira, R. A.; Santilli, C. V.; Craievich, A. F. *J. Mater. Chem.* **2001**, *11*, 3249. (i) Carlos, L. D.; Sá Ferreira, R. A.; Orion, I.; de Zea Bermudez, V.; Rocha, J. *J. Luminescence* **2000**, *87*−*89*, 702.

(17) Ribeiro, S. J. L.; Dahmouche, K.; Ribeiro, C. A.; Santilli, C. V.; Pulcinelli, S. H. J. *J. Sol-Gel Sci. Technol.* **1998**, *13*, 427.

(18) (a) Bekiari, V.; Lianos, P.; Stangar, U. L.; Orel, B.; Judeinstein, P. *Chem. Mater.* **2000**, *12*, 3095. (b) Bekiari, V.; Pistolis, G.; Lianos, P. *J. Non-Cryst. Solids* **1998**, *226*, 200. (c) Bekiari, V.; Pistolis, G.; Lianos, P. *Chem. Mater.* **1999**, *11*, 3189. (d) Bekiari, V.; Lianos, P.; Judeinstein, P. *Chem. Phys. Lett.* **1999**, *307*, 310.

(19) (a) Armand, M.; Poinsignon, C.; Sanchez, J.-Y.; de Zea Bermudez, V. U. S. Pat. 5,283,310, 1994. (b) de Zea Bermudez, V.; Poinsignon, C.; Armand, M. *J. Mater. Chem.* **1997**, *7* (9), 1677.

(20) (a) Gonçalves, M. C.; de Zea Bermudez, V.; Ostrovskii; D.; Carlos, L. D. *Ionics* **2002**, *8* (1&2), 62. (b) Dahmouche, K.; Gonçalves, M. C.; Santilli, C. V.; de Zea Bermudez, V.; Carlos, L. D.; Craievich, A. *Nucl. Instrum. Methods Phys. Res., Sect. B* **2003**, *199*, 117.

(21) Carlos, L. D.; Sá Ferreira, R. A.; de Zea Bermudez, V., Ribeiro, S. J. L. *Adv. Funct. Mater.* **2001**, *11* (2), 111.

Scheme 1. Synthetic Procedure of the d-Ut(300)$_n$Eu(CF$_3$SO$_3$)$_3$ Di-Urethanesils

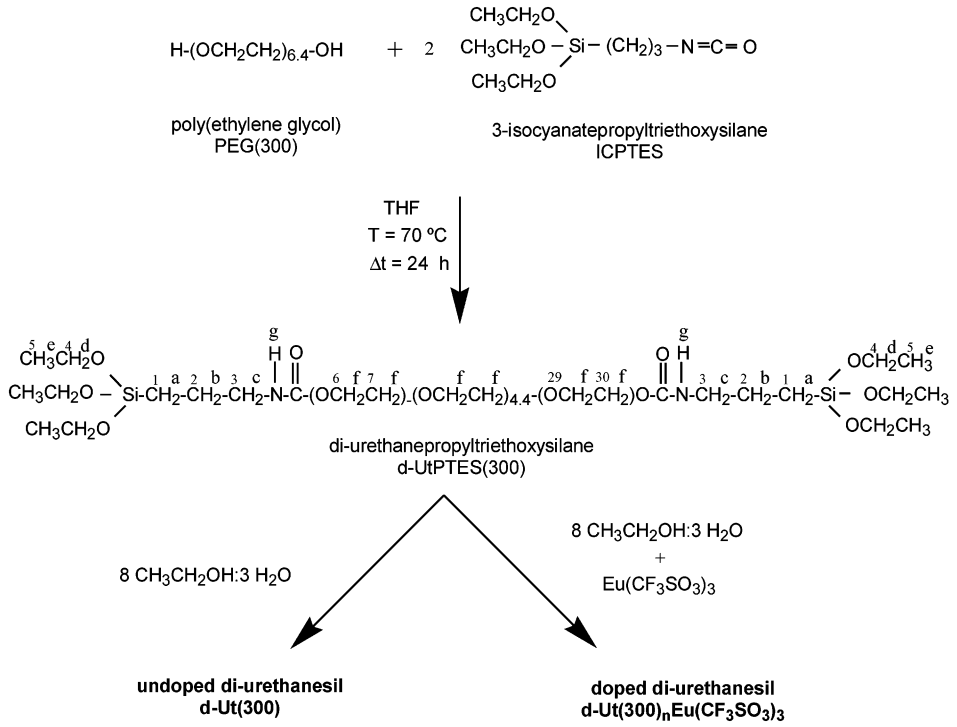

Table 1. Relevant Details of the Synthetic Procedure of the d-Ut(300)$_n$Eu(CF$_3$SO$_3$)$_3$ Di-Urethanesils

host matrix		d-Ut(300)
	Step 1	
	mPEG (300)/g	1.5
	v(ICPTES)/mL	2.469
	v(THF)/mL	10
	Step 2	
	v(H_2O)/μL	270
	v(CH_3CH_2OH)/mL	2.339

n	m(Eu(CF$_3$SO$_3$)$_3$) (g)	Si/Eu^{3+} (mol/mol)	Si/Eu^{3+} (g/g)
400	0.048	124.8	23.07
200	0.096	62.4	11.53
100	0.192	31.2	5.77
90	0.213	28.1	5.20
80	0.240	25.0	4.61
70	0.274	21.8	4.04
60	0.320	18.7	3.46
50	0.384	15.6	2.88
40	0.480	12.5	2.31
30	0.640	9.4	1.73
20	0.960	6.2	1.15
10	1.920	3.1	0.58
5	3.840	1.5	0.29
2	9.600	0.6	0.12
1	19.201	0.3	0.06

H^d), 3.72−3.58 (m, 26 H, H^f), 3.17−3.12 (m, 4 H, H^c), 1.63−1.55 (m, 4 H, H^b), 1.22−1.18 (m, 18 H, H^e), 0.62−0.58 (m, 4 H, H^a). ^{13}C NMR ($CDCl_3$, 100.62 MHz) δ (ppm) 156.16 (C=O), 77.32−63.40 (C^6−C^{30}), 58.06 (C^4), 43.11 (C^3), 22.96 (C^2), 17.94 (C^5), 7.29 (C^1).

Step 2. Synthesis of the di-Urethanesil Hybrid Xerogels, d-Ut(300)$_n$Eu(CF$_3$SO$_3$)$_3$ (Scheme 1). A volume of 2.339 mL of CH_3CH_2OH, an appropriate mass of Eu(CF$_3$SO$_3$)$_3$ (Table 1), and 270 μL of H_2O were added to the d-UtPTES(300) solution prepared in the first stage of the synthetic procedure (molar proportion 1:4:1.5 ICPTES/CH_3CH_2OH/H_2O). The mixtures were stirred in a sealed flask for 30 min and then cast into a Teflon mold, which was covered with Parafilm and left in a fume cupboard for 24 h. After a few hours gelation was already visible. The mold was transferred to an oven at 60 °C and the sample was aged for a period of 2 weeks. A transparent monolithic bulk was thus formed.

Experimental Techniques. The ^{1}H and ^{13}C NMR spectra were recorded in $CDCl_3$ on a Bruker ARX400 NMR spectrometer (400.13 and 100.62 MHz, respectively) at CACTI−Universidad de Vigo (Spain). Chemical shifts are quoted in ppm from tetramethylsilane (TMS). The abbreviations m, s, and b denote multiplet, singlet, and broad, respectively.

^{29}Si MAS and ^{13}C cross-polarization (CP) MAS NMR spectra were recorded on a Bruker Avance 400 (9.4 T) spectrometer at 79.49 and 100.62 MHz, respectively. ^{29}Si MAS NMR spectra were recorded with 2-μs (equivalent to 30°) rf pulses, a recycle delay of 60 s, and at a 5.0-kHz spinning rate. ^{13}C CP/MAS NMR spectra were recorded with 4-μs ^{1}H 90° pulse, 2-ms contact time, a recycle delay of 4 s, and at a spinning rate of 8 kHz. Chemical shifts are quoted in ppm from TMS.

The XRD measurements were performed at RT with a Rigaku Geigerflex D/max-c diffractometer system using monochromated Cu Kα radiation (λ = 1.54 Å) over the 2θ range of 4 to 80° at a resolution of 0.05°. The xerogel samples, analyzed as films, were not submitted to any thermal pretreatment.

The FT-IR spectra of the di-urethanesil samples were acquired at RT using a Unicam FT-IR system. The spectra were collected over the range 4000−400 cm^{-1} by averaging 60 scans at a maximum resolution of 1 cm^{-1}. The compounds were finely ground (about 2 mg), mixed with approximately 175 mg of dried potassium bromide (Merck, spectroscopic grade), and pressed into pellets. Prior to recording the spectra the disks were stored in an oven under vacuum at 90 °C for several days to reduce the levels of adsorbed water.

The FT-Raman spectra were recorded at RT with a Bruker IFS-66 spectrometer equipped with a FRA-106 Raman module and a near-infrared YAG laser with wavelength 1064 nm. The spectra were collected over the 3200−300 cm^{-1} range at a resolution of 2 cm^{-1}. The accumulation time for each spectrum was 4 h.

PL and PLE spectra were measured between 10 K and RT on a Jobin Yvon-Spex spectrometer (HR 460) coupled to a R928 Hamamatsu photomultiplier. A Xe arc lamp (150 mW) coupled to a Jobin Yvon-Spex monochromator (TRIAX 180) was used as excitation source. All the spectra were corrected for the response of the detector. The lifetime measurements were carried out at 10 K using a pulsed Xe arc lamp (5 mJ/pulse,

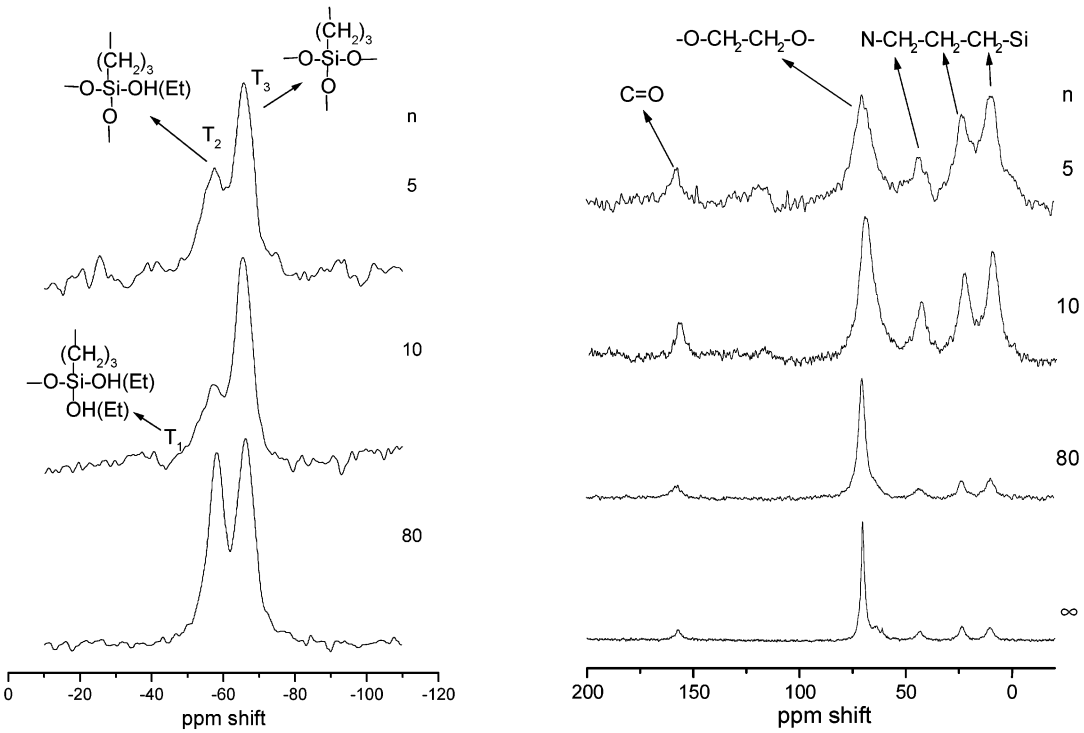

Figure 1. ^{29}Si MAS (left) and ^{13}C CP/MAS (right) NMR spectra of selected d-Ut(300)$_n$Eu$(CF_3SO_3)_3$ di-urethanesils.

3-μs bandwidth) coupled to a Kratos GM-252 monochromator and a Spex 1934 C phosphorimeter.

The absolute emission quantum yields, ϕ, were measured at RT according to the experimental technique for powdered samples described by Wrighton et al.[22] and were calculated as $\phi = A/(R_s - R_H)$, where A is the area under the di-urethanesil′ emission spectrum, and R_S and R_H are the diffuse reflectance − with respect to a fixed wavelength − of the hybrid and of the reflecting standard, respectively. The emission and diffuse reflectance spectra were corrected for the detector spectral response. The reflecting standard used was magnesium oxide (MgO) which has a reflectivity close to the unit (r = 91%). In the experimental method adopted, the powder size and packing fraction are crucial factors, because R_S and R_H intensity depend on them. Taking this aspect into account, the diffuse reflectance was first measured at a wavelength not absorbed by the nanohybrids (720 nm). The di-urethanesil material was thoroughly ground until R_H totally overlapped R_S, indicating a similar powder size and packing fraction. To prevent insufficient absorption of the exciting radiation, a powder layer around 3 mm was used and utmost care was taken to ensure that only the sample was illuminated in order to diminish the quantity of light scattered by the front sample holder. The diffuse reflectance and emission spectra were detected with the photoluminescence equipment described above, using a perpendicular illumination of the sample. The same experimental conditions (namely, the position of the hybrid/standard holder, the excitation and detection monochromator slits (0.2 and 0.1 mm, respectively), and the optical alignment) were kept constant in all the measurements. The errors in the quantum yield values associated with this technique were estimated to be around 25%.[22] The accuracy and reproducibility of our measurements were tested measuring the ϕ value of sodium salicylate (Panreak, 99.5%), a commercial standard. This compound presents a large broad band peaking around 425 nm, with a constant ϕ value (60%) for excitation wavelengths between 220 and 380 nm. These properties render sodium salicylate an adequate standard for ultra-violet absorbing samples, such as the di-urethanesil hybrids. Five measurements were performed to determine the sodium salicylate quantum yield at 350 nm, using the experimental setup described. The values found are within the 65.9 ± 3.6% interval.

(22) Wrighton, M. S.; Ginley, D. L.; Morse, J. *J. Phys. Chem.* **1974**, *78*, 2229.

Table 2. ^{29}Si NMR Chemical Shifts (±0.3 ppm), Population (±5 %) of the Different T_n Species, and Degree of Condensation, C, of the Selected d-Ut(300)$_n$Eu$(CF_3SO_3)_3$ Di-Urethanesils

	T_1		T_2		T_3			
	shift		shift		shift			
n	(ppm)	(%)	(ppm)	(%)	(ppm)	(%)	c (%)	formula[a]
80	−53.5	7	−58.2	40	−66.1	53	82	$R'_{0.5}Si(OR)_{0.54}O_{1.23}$
10	−53.1	10	−57.9	22	−65.6	68	86	$R'_{0.5}Si(OR)_{0.42}O_{1.29}$
5	−52.7	6	−57.6	34	−65.7	60	85	$R'_{0.5}Si(OR)_{0.46}O_{1.27}$

[a] R = −H or $-CH_2CH_3$.

III. Results and Discussion

Structure. Figure 1 (left) shows the ^{29}Si MAS NMR spectra of representative samples of the d-Ut(300)$_n$Eu-$(CF_3SO_3)_3$ di-urethanesil family. These spectra exhibit three distinct signals at about −53, −58, and −66 ppm (Figure 1 (left)). According to the conventional T_m notation, where m (m = 1, 2, 3) is the number of silicon-bridging oxygen atoms, these peaks are assigned to T_1, T_2, and T_3 units, respectively. It is worth noting that in the spectra of the three samples the signal produced by the T_1 site is almost negligible (Figure 1 (left)). In the case of the less concentrated sample (n = 80) the signals due to T_2 and T_3 have approximately the same intensity, whereas in the materials with n = 10 and 5 the amount of T_2 species is about half of that corresponding to the T_3 environments (Figure 1 (left)). The calculated relative proportions of the various silicon sites (quantitatively estimated through curve-fitting) and the polycondensation ratio c (where $c = {}^1/_3(\%T_1 + 2\%T_2 + 3\%T_3)$) of the three xerogels examined are collected in Table 2. These data support the claim that in this set of samples the main environment present is the T_3 site, typically

associated with the existence of functional $-(CH_2)_3SiO_{3/2}$ groups, a proof that the condensation process favored branched structures rather than linear segments. The *c* values determined for d-Ut(300)$_n$Eu$(CF_3SO_3)_3$ ($n = 80$, 10, and 5) are salt-concentration independent and are identical to that obtained for the corresponding nondoped framework.[16i] It is important to stress that the polycondensation ratios calculated here are of the same order of magnitude as those reported for the nondoped di-ureasils[16i] and for other Eu^{3+}-containing hybrid xerogels reported in the literature.[23]

The three peaks centered at about 43.5, 23.0, and 10.3 ppm in the ^{13}C CP/MAS NMR spectra of the d-Ut(300)-based samples with $n = \infty$, 80, 10, and 5 reproduced in Figure 1 (right) are attributed to the C^3, C^2, and C^1 carbon atoms of the propyl chains, respectively. This assignment is consistent with that proposed by Franville et al.[23] and Chang et al.[24] The three signals mentioned above appear at approximately the same position as those produced by the corresponding methylene groups of the propyl segments of the d-UtPTES(300) parent precursor (Experimental Section). On the basis of Ribot et al.'s[25] assignment, the peak observed near 70.0 ppm in the four ^{13}C CP/MAS NMR spectra shown in Figure 1 (right) is attributed to the CH_2 groups of the POE chains. This peak corresponds to that found between 77.32 and 63.40 ppm in the ^{13}C NMR spectrum of d-UtPTES(300) (Experimental Section). Finally, the signal seen at 157.6 ppm in the ^{13}C CP/MAS NMR spectra of the di-urethanesils studied in the present work (Figure 1 (right)) is associated with the carbon atom of the C═O group of the urethane linkage.[23] In the ^{13}C NMR spectrum of the non-hydrolyzed d-UtPTES-(300) precursor this signal is detected at 156.16 ppm (Experimental Section).

The ^{13}C CP/MAS NMR data demonstrate that no modifications of the Si-bonded propyl chains, POE segments, or cross-links occurred during the second stage of the synthetic procedure of the d-Ut(300)$_n$Eu-$(CF_3SO_3)_3$ composites which involved the typical sol−gel reactions, i.e., the hydrolysis and condensation reactions. The characteristic peaks of the ethoxy groups, at 58.06 and 17.94 ppm in the ^{13}C liquid-state NMR spectrum of d-UtPTES(300) (Experimental Section) and quoted at 58.1 and 17.6 ppm by Nahhal et al.,[26] are only seen in the ^{13}C CP/MAS NMR spectra of the d-Ut-(300)$_n$Eu$(CF_3SO_3)_3$ $n = \infty$ and 80 (broad peak) xerogels (Figure 1 (right)). In fact we may deduce from the ^{29}Si MAS data that in the final materials a minor number of ethoxy/hydroxy groups remain bonded to the silicon atoms (Table 2).

The empirical formula deduced on the basis of the ^{29}Si and ^{13}C MAS NMR spectra of the d-Ut(300)-based samples (Table 2) leads us to suggest that the structure of the di-urethanesils may be tentatively represented in Scheme 2.

The integrated intensity and full-width-at-half-maximum (fwhm) of the ^{13}C NMR resonances were obtained by fitting the ^{13}C CPMAS spectra (Figure 1 (right)) with Lorentzian−Gaussian functions. The through-space dipolar interaction between the ^{13}C nuclei and the paramagnetic Eu^{3+} centers results in significant changes in the ^{13}C CPMAS NMR spectra of Eu^{3+}-doped materials. When *n* decreases from ∞ to 5, the integrated areas of the OCH_2CH_2O (70 ppm) and C═O resonances (158 ppm) drop by a factor of, respectively, 3.9 and 2.3 relative to the areas of the propyl chains peaks (at ca. 44, 23, and 10 ppm). Concomitantly, the fwhm of the resonances increases (from $n = \infty - 5$): OCH_2CH_2O, 2 to 9.6 ppm; C═O, 4.8 to 10.8 ppm. The ^{13}C nuclei of functional groups directly linked to Eu^{3+} give NMR resonances broadened beyond detection and, thus, the C═O peaks observed in the ^{13}C CPMAS spectra indicate the presence of non-hydrogen-bonded C═O groups (noncoordinated to Eu^{3+}) in di-urethanesils with $n \geq 5$. The relatively small broadening and intensity decrease of the C═O and OCH_2CH_2O peaks, observed upon increasing the lanthanide concentration in the materials, is not due to coordination of Eu^{3+} but rather to the presence of such ions a few angstroms away.

The diffractograms of the d-Ut(300)$_n$Eu$(CF_3SO_3)_3$ materials reproduced in Figure 2 reveals that the compounds with $\infty \geq n \geq 10$ are totally amorphous. The broad peak centered around 21.60° in the XRD patterns of the latter xerogels is ascribed to the coherent diffraction of the siliceous backbone of the nanohybrids.[27] The structural unit distance, calculated using the Bragg law, is approximately 4.11 Å. The weak broad hump clearly distinguished in the diffractogram of the d-Ut(300)$_{10}$Eu-$(CF_3SO_3)_3$ sample at ca. 40−45° might be due to the second-order of the peak at ca. 21−22° (Figure 2). The absence of any crystalline regions in these samples correlates well with the presence of low-molecular-weight POE chains in the host organic/inorganic framework.

The diffractograms of d-Ut(300)$_5$Eu$(CF_3SO_3)_3$ (not shown) and d-Ut(300)$_1$Eu$(CF_3SO_3)_3$ (Figure 2) demonstrate that further addition of triflate salt to d-Ut(300) gives rise to the growth of several diffraction peaks whose locations coincide exactly with the positions of the characteristic peaks of crystalline $Eu(CF_3SO_3)_3$.

Scheme 2. Representation of the Structure of the d-Ut(300)$_n$Eu$(CF_3SO_3)_3$ Di-Urethanesils.

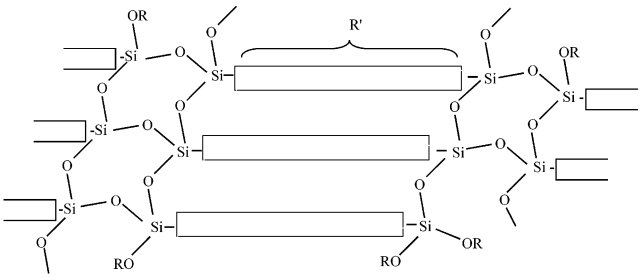

R'= -$(CH_2)_3$-NH-C(=O)-$(OCH_2CH_2)_6$-O-C(=O)-NH-$(CH_2)_3$-

R = -H or -CH_2CH_3

Note: The ratio T_1:T_2:T_3 in this scheme does not correspond to those given in Table 2. A T_1 site has been represented for the sake of clarity.

(23) Franville, A.-C.; Mahiou, R.; Zambon, D.; Troin Y.; Cousseins, J.-C. *Solid State Sci.* **2001**, *3*, 211

(24) Chang, T. C.; Wang, G. P.; Tsai, H. C.; Hong, Y. S.; Chiu, Y. S. *Polym. Degrad. Stab.* **2001**, *74*, 229.

(25) Ribot, F.; Lafuma, A.; Eychenne-Baron, C.; Sanchez, C. *Adv. Mater.* **2002**, *14*, 1496.

(26) El Nahhal, I. E.; Chehimi, M. M.; Cordier, C.; Dodin, G. *J. Non-Cryst. Solids* **2000**, *275*, 142.

(27) Carlos, L. D.; de Zea Bermudez, V.; Sá Ferreira, R. A.; Marques, L.; Assunção, M. *Chem. Mater.* **1999**, *11* (3), 581.

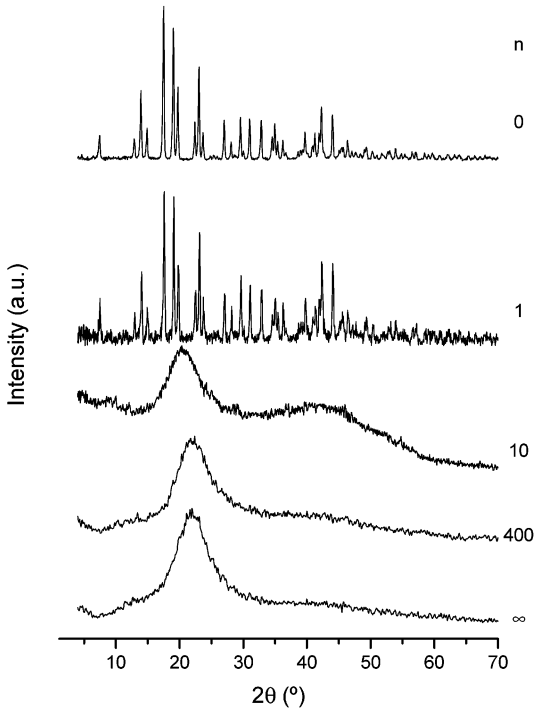

Figure 2. XRD patterns of selected d-Ut(300)$_n$Eu(CF_3SO_3)$_3$ di-urethanesils.

These findings lead us to conclude not only that free salt occurs in samples with $n \leq 5$, but also that neither crystalline POE/Eu(CF_3SO_3)$_3$ complexes, nor pure crystalline POE phases, are formed throughout the range of salt concentrations investigated.

FT-IR and FT-Raman Spectra. To find additional proof of the absence of crystalline domains of POE and/or POE-based complexes in the di-urethanesils examined here, and especially to investigate the nature of the first coordination sphere of the cations and the local chemical environment of the anions, we decided to inspect the FT-IR spectra of the d-Ut(300)$_n$Eu(CF_3SO_3)$_3$ nanohybrids in the CO stretching (νCO) and "amide I" regions and the corresponding FT-Raman spectra in the region characteristic of the symmetric stretching mode of the SO_3 group ($\nu_s SO_3$).

The RT FT-IR spectra of the materials with $\infty \geq n \geq 5$ in the 1400−770 cm^{-1} region is represented in Figure 3. Comparison of these spectra with that of liquid hexa(ethylene glycol) dimethyl ether (HEGDME, $CH_3O(CH_2CH_2O)_6CH_3$)[28a] is of interest to determine the degree of disorder of the uncomplexed POE chains of the hybrid xerogels under study. Matsuura et al.[28b] associated the events located at 1326 (weak), 992 (weak), 915 (shoulder), and 810 (shoulder) cm^{-1} in the infrared spectrum of liquid high-molecular-weight poly(ethylene glycol) (PEG) to the molten or amorphous state. In the spectrum of the HEGDME oligomer two features characteristic of the liquid state were observed at 1330 and 985 cm^{-1}.[28a] However, the detection of this pair of events in the spectra of the d-Ut(300)$_n$Eu(CF_3SO_3)$_3$ samples is complicated. Whereas the 1330 cm^{-1} band is masked by the broad envelope due to the asymmetric stretching vibration of the SO_3 group of the triflate ion, which spans wavenumbers from approximately 1340 to 1230 cm^{-1}, the 985 cm^{-1} feature is too ill-defined to serve as the only proof of the existence of amorphous POE chains (Figure 3). A more unambiguous and straightforward diagnostic band of the liquid state in PEG is the medium-intensity event centered at approximately 1354 cm^{-1}, which corresponds to the bands located at 1364 and 1345 cm^{-1} in the spectrum of crystalline PEG.[28c] The 1354 cm^{-1} band, ascribed to the CH_2 wagging vibration mode,[28b] is clearly seen in the spectra of the d-Ut(300)$_n$Eu(CF_3SO_3)$_3$ materials (Figure 3). Its presence unequivocally supports the suggestion that the free POE chains of the hybrid framework are totally amorphous in the range of salt compositions examined, a result that corroborates the XRD data.

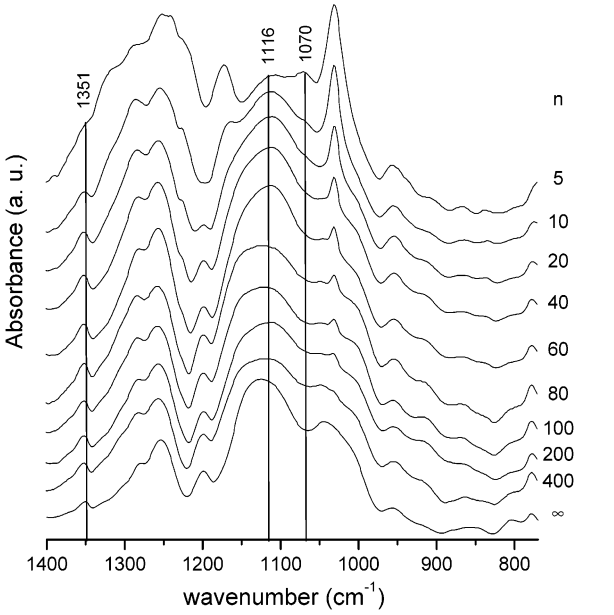

Figure 3. FT-IR spectra of selected d-Ut(300)$_n$Eu(CF_3SO_3)$_3$ di-urethanesils in the νCO region.

It is known that the νCO mode of POE is an excellent tool to probe the changes undergone by the polymer chains of the hybrids upon incorporation of the guest salt. In this spectral region (1190−1050 cm^{-1}) the complexation of the cations by the oxygen atoms of the polyether chains induces a distinct shift of the strong νCO band to lower wavenumbers. The fact that the 1116 cm^{-1} feature of the nondoped di-urethanesil matrix, characteristic of noncoordinated oxyethylene moieties,[28a] remains practically unchanged in the spectra of all the di-urethanesils examined (curve-fitting results not shown and ref 20a) may be interpreted as an evidence that, regardless of the Eu(CF_3SO_3)$_3$ content, there are POE chains of the host structure which persist in an uncomplexed state.[20a] The new event that emerges as a shoulder near 1069 cm^{-1} in the spectrum of d-Ut(300)$_{10}$Eu(CF_3SO_3)$_3$ (Figure 3) and is transformed into a strong band in the spectrum of the salt-rich material with $n = 5$ (Figure 3) is attributed to Eu^{3+}-coordinated ether oxygen atoms,[20a,29−31] a suggestion that the com-

(28) (a) Machida, K.; Miyazawa, T. *Spectrochim. Acta* **1964**, *20*, 1865. (b) Matsuura, H.; Miyazawa, T. *J. Polym. Sci.* **1969**, *7* (A-2), 1735. (c) Matsuura, H.; Miyazawa, T.; Machida, K. *Spectrochim. Acta* **1973**, *29A*, 771.

(29) Bernson, A.; Lindgren, J. *Solid State Ionics* **1993**, *60*, 31.

(30) de Zea Bermudez, V.; Ostrovskii, D.; Gonçalves, M. C.; Carlos, L. D.; Sá Ferreira, R. A.; Reis, L.; Jacobsson, P. *Phys. Chem. Chem. Phys.* **2004**, *6* (3), 638.

plexation of the cations by the POE chains takes place in materials with $n \leq 10$. We must note, however, that thermal data (unpublished) suggest that the beginning of the cation/POE interaction may occur at a slightly higher composition (i.e., lower salt concentration) than that deduced from spectroscopic data. In fact, it is very likely that the 1069 cm^{-1} band is masked by the strong 1116 cm^{-1} feature in the FT-IR spectrum of a slightly less concentrated sample. No characteristic bands of a crystalline $POE_nEu(CF_3SO_3)_3$ complex[30] are discerned in the νCO region of the d-Ut$(300)_5Eu(CF_3SO_3)_3$ xerogel, supporting the conclusions drawn from the XRD analysis.

The FT-Raman spectra of the di-urethanesils with $n \geq 5$ in the 925−780 cm^{-1} region previously reported[20a] complement the information retrieved from the FT-IR spectra. The prominent band observed at approximately 860 cm^{-1} in the FT-Raman spectrum of the di-urethanesil xerogel with $n = 5$ was considered as a solid piece of evidence of the interaction established between the lanthanide ions and the ether oxygen atoms of the POE chains in the d-Ut$(300)_5Eu(CF_3SO_3)_3$ composite.[20a] The 860 cm^{-1} event, ascribed to a stretching vibration mode involving wrapping of the POE segments around the Eu^{3+} ions,[32] is associated with a gauche conformation of the −O−C−C−O− bonds.[33] The feature discerned in the spectra of the doped di-urethanesils with $400 \geq n \geq 10$ at 813 cm^{-1}, attributed to the trans conformations of the −O−C−C−O− moieties,[33] practically disappeared at $n = 5$.[20a]

The FT-IR and FT-Raman spectroscopic results just discussed indicate that the first signs of the involvement of the ether oxygen atoms in the coordination of the Eu^{3+} ions are seen at $n = 10$. This conclusion implies that in the di-urethanesil hybrids with $n > 10$, the Eu^{3+} ions bond either to the carbonyl oxygen atoms of the urethane cross-links or to the triflate oxygen atoms, or to both types of donor atoms. It is useful to recall that in the complexes formed between POE and lanthanum triflate[34a] or europium bromide[34b,c] the coordination number of the lanthanide ion is 12.

To evaluate the role played by the urethane cross-links in the coordination of the Eu^{3+} ions we will analyze the spectral signature of the d-Ut$(300)_nEu(CF_3SO_3)_3$ xerogels in the "amide I" region. The "amide I" mode (or simply the carbonyl stretching mode) is a very complex vibration that receives a major contribution from the C═O stretching.[35a] As the C═O stretching vibration is sensitive to the specificity and magnitude of hydrogen bonding, the "amide I" envelope is usually a broad band that may be resolved into various components associated with different chemical environments of the C═O groups, usually designated as associations, aggregates, or structures. Quantitative analysis is possible in the "amide I" region only if the difference in the absorption coefficients of the nonbonded and bonded carbonyl bands is taken into account. Band area calculations may be thus considered as indicative of functional group concentration.[35]

Curve-fitting of the FT-IR spectra of selected d-Ut$(300)_nEu(CF_3SO_3)_3$ di-urethanesils was carried out in the 1825−1600 cm^{-1} interval using Gaussian band shapes (Figure 4 (top)). Three distinct components centered at about 1750, 1720, and 1696 cm^{-1} were found in the "amide I" envelope of the d-Ut(300) xerogel (Figure 4 (top)). In accordance with previous works,[20a,30,31] the 1750 cm^{-1} feature is assigned to urethane linkages in which N−H and C═O groups are nonbonded. The 1720 cm^{-1} band is attributed to the absorption of hydrogen-bonded C═O groups in disordered aggregates (e.g., polyether/urethane association), whereas the band located at 1696 cm^{-1} is associated with the absorption of C═O groups belonging to a considerably more ordered hydrogen-bonded aggregate (e.g., urethane/urethane association).[20a,30,31]

Although, as expected,[20a,30,31] the position of the three "amide I" components of the nondoped material is unaffected by the presence of the lanthanide salt, the addition of $Eu(CF_3SO_3)_3$ to d-Ut(300) has several consequences in the "amide I" region (Figure 4 (top)). Apart from changes in the intensity of these three components, at $n = 60$ a new event emerges around 1666 cm^{-1} as a shoulder, which is transformed into the most intense band of this spectral interval in compounds with $n = 5$ and 1. In addition, at $n = 1$ a new component is detected at 1635 cm^{-1}.

These spectral data demonstrate that the Eu^{3+} ions interact with the carbonyl oxygen atoms of the urethane cross-links in samples with $n \geq 1$, a result that enlarges the range of concentrations previously determined for this particular cation coordinating situation.[20a] To examine this effect quantitatively, we calculated the composition dependence of the area of the 1750, 1720, 1696, 1666, and 1635 cm^{-1} components.

Close analysis of the plot obtained (Figure 4 (bottom)) allows us to conclude that in samples with $\infty > n \geq 60$ the introduction of increasing amounts of salt leads to the regular decrease of the proportion of nonbonded C═O groups. In the same composition range the fraction of urethane−urethane aggregates is maintained nearly constant, whereas the amount of polyether/urethane aggregates in the xerogel with $n = 100$ increases slightly with respect to that found in d-Ut(300) and then remains practically unchanged up to $n = 60$ (Figure 4 (bottom)).

In samples with $n < 60$ dramatic modifications take place as the europium salt content rises (Figure 4 (bottom). (1) While the proportion of nonbonded C═O groups continues to decrease smoothly, the fraction of POE/urethane aggregates and urethane/urethane associations suffers a reduction, which is particularly abrupt at $n < 20$, an indication that these hydrogen-bonded aggregates are massively destroyed. In the most

(31) Gonçalves, M. C.; de Zea Bermudez, V.; Ostrovskii, D.; Carlos, L. D. *J. Mol. Struct.* **2002**, *611* (2−3), 83.

(32) (a) Papke, B. L.; Ratner, M. A.; Shriver, D. F. *J. Phys. Chem. Solids* **1981**, *42*, 493. (b) Papke, B. L.; Ratner, M. A.; Shriver, D. F. *J. Electrochem. Soc.* **1982**, *129* (7), 1434. (c) Ericson, H.; Mattson, B.; Torell, L. M.; Rinne, H.; Sundholm, F. *Electrochim. Acta* **1998**, *43* (10−11), 1401. (d) Furlani, M.; Ferry, A.; Franke, A.; Jacobsson, P.; Mellander, B.-E. *Solid State Ionics* **1998**, *113−115*, 129. (e) Brodin, A.; Mattson, B.; Nilsson, K.; Torell, L. M.; Hamara, J. *Solid State Ionics* **1996**, *85*, 111.

(33) (a) Sato, H.; Kusumoto, Y. *Chem. Lett.* **1978**, 635. (b) Maxfield, J.; Shepherd, I. W. *Polymer* **1975**, *16*, 505. (c) Matsuura, H.; Fukuhara, K. *J. Mol. Struct.* **1985**, *126*, 251.

(34) (a) Bernson, A.; Lindgren, J.; Huang, W.; Frech, R. *Polymer* **1995**, *36* (23), 4471. (b) Carlos, L. D.; Videira, A. L. L. *Chem. Phys. Lett.* **1997**, *264*, 57. (c) Videira, A. L. L.; Carlos, L. D. *J. Chem. Phys.* **1996**, *105*, 8878.

(35) (a) Skrovanek, D. J.; Howe, S. E.; Painter, P. C.; Coleman, M. M. *Macromolecules* **1985**, *18*, 1676. (b) Coleman, M. M.; Lee, K. H.; Skrovanek, D. J.; Painter, P. C. *Macromolecules* **1986**, *19*, 2149.

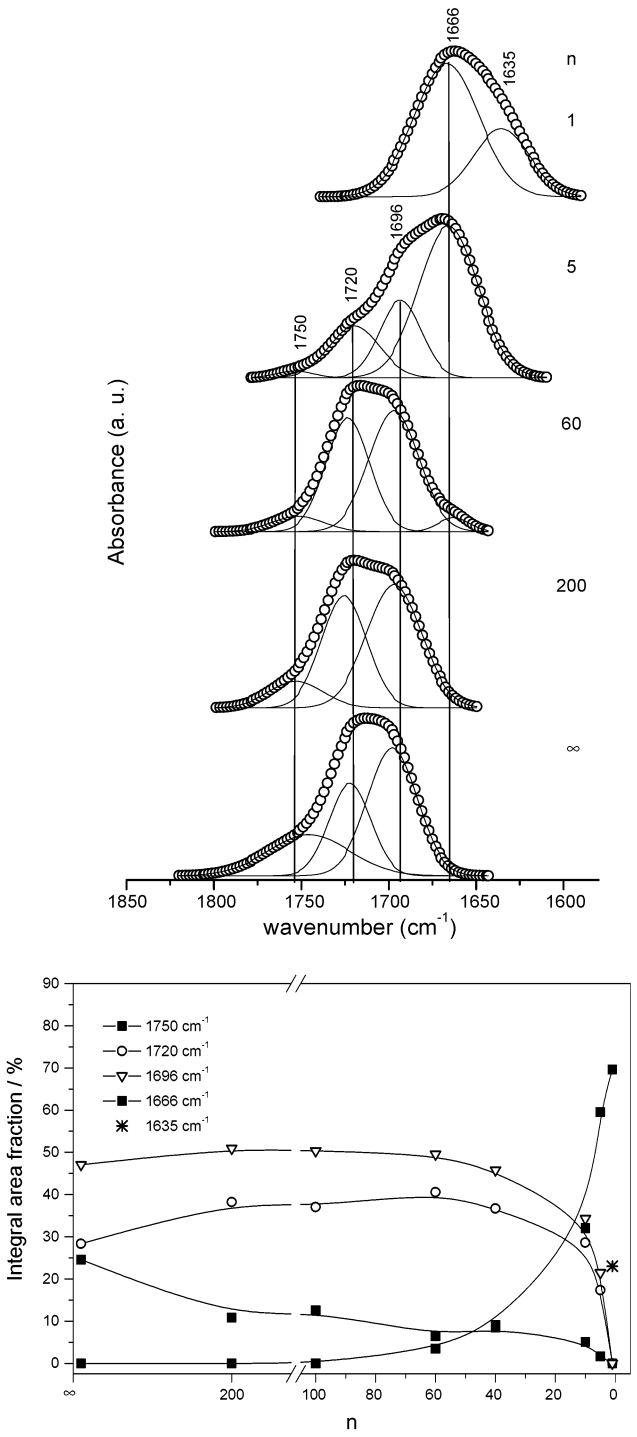

Figure 4. "Amide I" region of selected d-Ut(300)$_n$Eu$(CF_3SO_3)_3$ di-urethanesils: (top) curve-fitting results of the FT-IR spectra and (bottom) salt-concentration dependence of the integral intensity of the different spectral components. The curves are guides for the eyes.

concentrated di-urethanesil examined ($n = 1$) the POE/urethane and urethane/urethane structures no longer exist and the saturation of the free C═O sites is attained. (2) The area of the 1666 cm^{-1} feature increases rapidly. On the basis of previous assignment,[30,31] the latter band is associated with highly ordered, strongly hydrogen-bonded aggregates, formed at the expense of the breakdown of all the previously existent ones. The regular increase of this band with the increase of salt content reveals that the new hydrogen-bonded aggregates formed are strongly coordinated to the Eu^{3+} ions.[30,31]

The conclusion derived from the analysis of the "amide I" region that non-hydrogen-bonded C═O groups exist in the di-urethanesils with $n \geq 5$ is consistent with the presence of the resonance peaks near 157.6 ppm in the ^{13}C MAS/CP NMR spectra (Figure 1 (right)), which supports the occurrence of free C═O groups (i.e., not involved in the coordination of the lanthanide ions).

We will now inspect in the FT-Raman spectra of the $Eu(CF_3SO_3)_3$-based composites the changes undergone by the ν_sSO_3 mode as a function of salt concentration to evaluate the cation−anion interactions established in the di-urethanesil medium.

The ν_sSO_3 mode of the "free" triflate ion appears at 1032 cm^{-1}.[36a] Upon coordination, the ν_sSO_3 band, which corresponds to a nondegenerate mode of the anion, may shift to higher wavenumbers,[36b,c,d,e] to lower wavenumbers,[36b,f] and to both higher and lower wavenumbers.[36d,g] In some cases, the ν_sSO_3 band remains unshifted.[36f]

The FT-Raman spectra of the di-urethanesils in the ν_sSO_3 region are shown in Figure 5 (left). The components isolated in the FT-Raman ν_sSO_3 profiles are depicted in Figure 5 (right). The FT-Raman ν_sSO3 envelope of the xerogels with $n > 60$ was resolved into two distinct components: a band at about 1031 cm^{-1} and a weak shoulder centered at approximately 1025 cm^{-1} (not shown). The ν_sSO3 band of the xerogels with $60 \geq n \geq 10$ was decomposed into three components: a peak at approximately 1031 cm^{-1} and two shoulders positioned around 1039 and 1024 cm^{-1} (Figure 5 (right)). In all the cases the intensity of the 1031 cm^{-1} feature is significantly higher than that of the shoulders. The spectra of the d-Ut(300)$_n$Eu$(CF_3SO_3)_3$ materials with $n = 5$ and 1 also display these three events. In addition, two new peaks located at 1047 and 1069 cm^{-1} and a pair of new shoulders centered at about 1052 and 1062 cm^{-1} can be seen (Figure 5 (right)). In the FT-Raman spectrum of d-Ut(300)$_5$Eu$(CF_3SO_3)_3$ the 1031 and the 1047 cm^{-1} bands are the most intense features of the ν_sSO_3 region. In that of the salt-rich sample d-Ut(300)$_1$Eu$(CF_3SO_3)_3$, the 1069 and 1047 cm^{-1} events are transformed into the strongest components of this spectral region, whereas the intensity of the 1031 cm^{-1} band is markedly reduced (Figure 5 (right)).

The appearance of the 1031 cm^{-1} band in the FT-Raman spectra of the doped di-urethanesils suggests the occurrence of "free" anions over the whole range of salt concentrations studied. It is worth mentioning that the 1031 cm^{-1} band, typically ascribed to "free" $CF_3SO_3^-$ ions, can be also due, in urethane cross-linked POE/siloxane hybrids, to the formation of the so-called *cross-link separated ion pairs*.[37] The shoulder observed in the same spectral interval in samples with $n > 60$ and the two components on both sides of the 1032 cm^{-1} feature

(36) (a) Johnston, D. H.; Shriver, D. F. *Inorg. Chem.* **1993**, *32*, 1045. (b) Bergström, P.- Å.; Frech, R. *J. Phys. Chem.* **1995**, *99*, 12603. (c) Chintapalli, S.; Quinton, C.; Frech, R.; Vincent, C. A. *Macromolecules* **1997**, *30*, 7472. (d) Petersen, G.; Torell, L. M.; Panero, S.; Scrosati, B.; Silva, C. J.; Smith, M. J. *Solid State Ionics* **1993**, *60*, 55. (e) Brodin, A.; Mattson, B.; Nilsson, K.; Torell, L. M.; Hamara, J. *Solid State Ionics* **1996**, *85*, 111. (f) Wendsjö, Å.; Lindgren, J.; Thomas, J. O.; Farrington, G. C. *Solid State Ionics* **1992**, *53*−*56*, 1077. (g) Petersen, G.; Brodin, A.; Torell, L. M.; Smith, M. J. *Solid State Ionics* **1994**, *72*, 165

(37) de Zea Bermudez, V.; Ostrovskii, D.; Lavoryk, S.; Gonçalves, M. C.; Carlos,L. D. *Phys. Chem. Chem. Phys.* **2004**, *6* (3), 649.

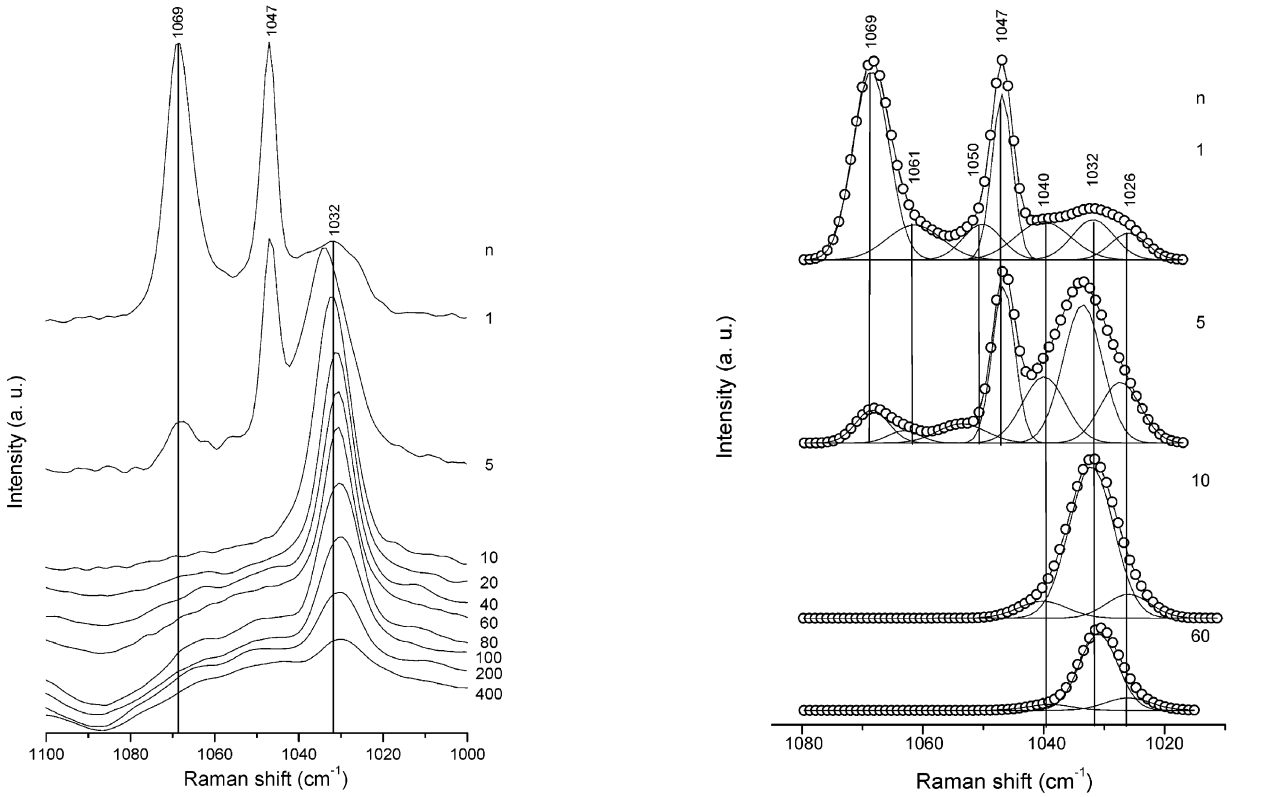

Figure 5. FT-IR spectra (left) and curve-fitting results (right) of d-Ut(300)$_n$Eu(CF_3SO_3)$_3$ di-urethanesils in the $\nu_s SO_3$ region. To examine exclusively the contribution of the $\nu_a SO_3$ mode, the spectrum of the pure polymer had to be first subtracted from those of the hybrids with 200 ≥ n ≥ 10. The wavenumbers indicated regard the values observed in the spectrum of the most concentrated sample.

detected in the case of the hybrids with 60 ≥ n ≥ 10 (Figure 5 (right)) are assigned to *weakly coordinated ion pairs*.[37] The component discerned at approximately 1047 cm^{-1} and the shoulders centered around 1052 and 1062 cm^{-1} at high salt concentration (n = 5 and 1) are associated with ionic aggregates. These species very likely involve the coordination of the cation to the oxygen atoms of the polymer chains.[37] The 1069 cm^{-1} band detected in spectra of xerogels with n = 5 and 1 is attributed to the occurrence of pure lanthanide salt.[37] The latter result is thus in perfect agreement with the XRD data obtained.

Photoluminescent Features and Chromaticity Diagram. Figure 6 reproduces the RT PLE spectra monitored within the $^7F_2$ emission lines for the d-Ut-(300)$_n$Eu(CF_3SO_3)$_3$ xerogels with n = 200, 10, and 5. The spectra are composed of a large broad band peaking around 345 nm, which is overlapped by a series of narrow lines corresponding to transitions between the $^7F_0$ and $^5H_4$, $^5D_4$, ^5G_J, $^5L_6$, $^5D_1$, $^5D_2$, and $^5D_3$ levels. The relative intensity between the band and the intra-4f^6 lines decreases as the Eu^{3+} content increases from n = 200 to 5. The presence of a large broad band in the PLE spectra monitored around the cation lines was already observed and reported for other classes of Eu^{3+}-based organic−inorganic hybrids, such as the Eu^{3+}-based di-ureasils.[16b,g] In accordance with previous assignment,[16b,g] this band will be ascribed to a ligand-to-metal charge transfer (LMCT) transition resulting from the interaction between the ligands and the lanthanide ions.

Figure 7 shows the RT PL spectra obtained for the d-Ut(300)$_{200}$Eu(CF_3SO_3)$_3$ recorded under different excitation wavelengths between 350 and 420 nm. All the

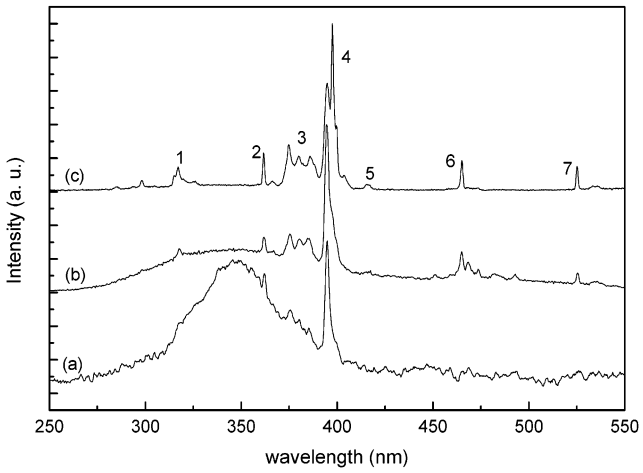

Figure 6. RT PLE spectra of the d-Ut(300)$_n$Eu(CF_3SO_3)$_3$ di-urethanesils: (a) n = 200, (b) n = 10, and (c) n = 5, monitored around the $^5D_0 \rightarrow {}^7F_2$ lines, 612−614 nm. (1), (2), (3), (4), (5), (6), and (7) denote the intra-4f ^{6} transitions: $^7F_0 \rightarrow {}^5H_4$, $^5D_4$, ^5G_J, $^5L_6$, and $^5D_{3-1}$, respectively.

spectra are composed of a large broad band between 380 and 650 nm, which is overlapped by a series of narrow lines in the orange-red spectral region. These lines are assigned to the Eu^{3+} intra-4f^6 transitions between the $^5D_0$ and the $^7F_{0-4}$ levels. The large broad band clearly presents two components: a main band in the blue spectral region, peaking between 450 and 475 nm, and a shoulder in the green spectral region, peaking around 505 nm. Only the energy of the former component depends on the selected excitation wavelength, in contrast to the less energetic band, the peak position of

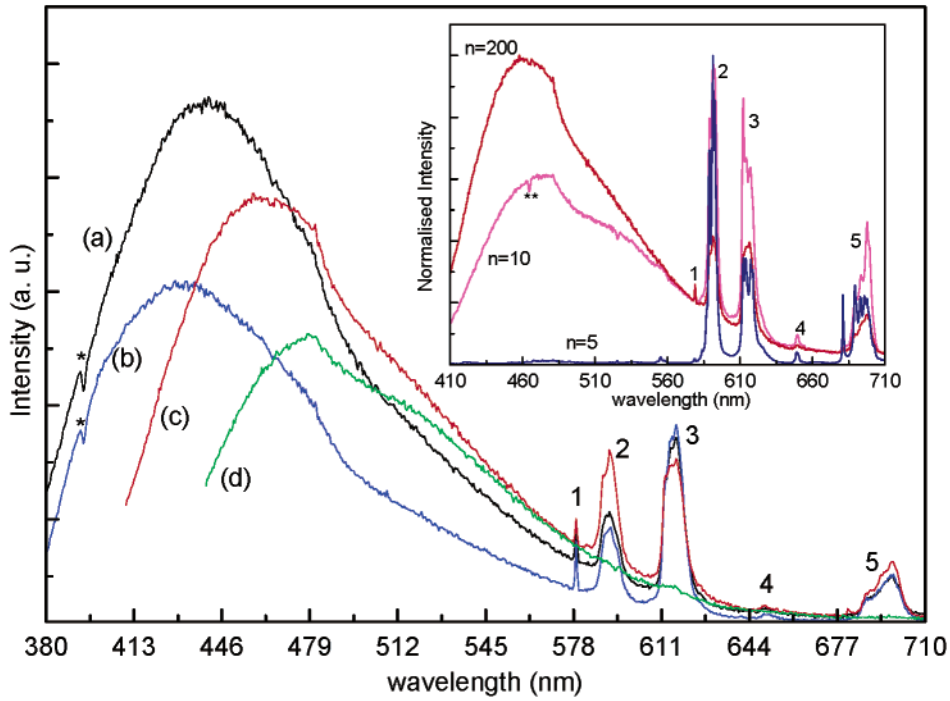

Figure 7. RT PL spectra of the d-Ut(300)$_{200}$Eu(CF_3SO_3)$_3$ di-urethanesils excited under different excitation wavelengths: (a) 350 nm, (b) 365 nm, (c) 395 nm, and (d) 420 nm. The inset shows the RT PL spectra excited under 395 nm for the di-urethanesils, d-Ut(300)$_n$Eu(CF_3SO_3)$_3$ with $n = 200$, 10, and 5. (1), (2), (3), (4), and (5) denote the intra-4f^6 transitions: $^5D_0 \rightarrow {}^7F_{0-4}$, respectively, and (*) and (**) indicate the intra-4f^6 self-absorptions $^7F_0 \rightarrow {}^5L_6$ and $^5D_2$, respectively.

which remains approximately the same in the entire excitation wavelength range between 350 and 420 nm. This band was previously detected in the nondoped hybrid (not shown) and it was also observed for other structurally similar hybrids (di-ureasils and mono-urethanesils).[15a,16,27] The green and blue components were assigned to radiative recombinations typical of donor−acceptor pairs, occurring in the NH groups of the grafting groups between the organic and inorganic phases (urea or urethane cross-links) and in the siliceous nanodomains, respectively.[16,27]

The relative intensity between the hybrid host's emission band and the Eu^{3+} cation lines strongly depends on the selected excitation wavelength and on the Eu^{3+} content. As Figure 7 demonstrates, in the most dilute hybrid ($n = 200$), the broad band and the Eu^{3+} lines can be clearly observed when the 350-nm excitation wavelength is used. When the higher 420-nm excitation wavelength is employed to irradiate the sample, only the large broad band could be detected. Increasing the Eu^{3+} concentration induces a decrease in the intensity of the host broad band associated with the cation lines, in such a manner that for $n = 5$ the hybrid host emission could hardly be detected (inset of Figure 7).

The relative intensity between the hybrid host's band and the Eu^{3+} lines upon changing the excitation wavelength or Eu^{3+} content can be quantitatively visualized through the calculation of the chromaticity (x, y) coordinates, according to the standard procedure defined by the Commission Internationale d'Éclairage (CIE).

Figure 8 displays the CIE chromaticity diagram where the (x, y) color coordinates of the d-Ut(300)$_n$(CF_3SO_3)$_3$ samples with $n = 200$, 10, and 5 are represented for excitation wavelengths within the 350−420 nm interval. As the diagram clearly shows, the color of the

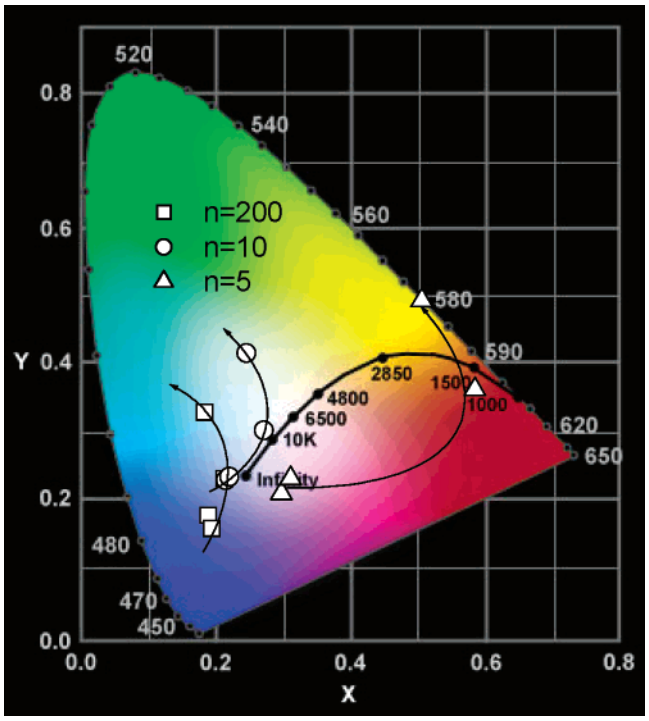

Figure 8. CIE chromaticity diagram showing the excitation-dependence of the RT (x, y) color coordinates for the d-Ut-(300)$_n$Eu(CF_3SO_3)$_3$ di-urethanesils with $n = 200$, 10, and 5. The arrows indicate variations in the excitation wavelength between 350 and 420 nm.

emission changes from the blue to the red spectral region with the increase in the Eu^{3+} content from $n = 200$ to 5, as a direct consequence of the enhancement of the Eu^{3+} emission lines, relative to the hybrid host broad band. Within each sample, an increase in the excitation wavelength from 350 to 420 nm induces

variations in the color coordinates. In particular, the color coordinates of the most dilute sample ($n = 200$) change from the blue (0.19, 0.18) to the blue-green region (0.18, 0.33) and the (x, y) coordinates of the emission of the most concentrated sample ($n = 5$) are shifted from the red-purple (0.30, 0.21) to the yellow (0.50, 0.49) spectral region. The luminescence of the d-Ut(300)$_{10}$Eu(CF_3SO_3)$_3$ compound is closer to the center of the diagram, where the white color region is defined. For the di-urethanesil with $n = 10$ the color coordinates change from the white region (0.22, 0.23) for the 350-nm excitation wavelength to the green region (0.25, 0.41) at the 420-nm excitation wavelength.

The dependence of the relative intensity between the hybrid host band and the Eu^{3+} emission lines is associated with the activation/deactivation of the energy-transfer processes that take place between the di-urethanesil emitting centers (donors) and the lanthanide ions (acceptors), as we show in the next section through the determination of the absolute emission quantum yields.

Room-Temperature Absolute Emission Quantum Yields. The di-urethanesils are versatile multi-wavelength emitters as clearly illustrated in the CIE chromaticity diagram of Figure 8. To quantify their emission efficiency and gain some information on the efficiency of the energy transfer processes, η, between the hybrid host (donor) and the metal ion (acceptor) it is crucial to determine the emission quantum yields. The efficiency of the energy transfer between the two species can be evaluated by measuring the absolute quantum yield in the presence (ϕ) and in the absence (ϕ_0) of the acceptor,[16g,38] as $\eta = 1 - (\phi/\phi_0)$. The ϕ value was measured for the d-Ut(300)$_n$Eu(CF_3SO_3)$_3$ hybrids with $n = 200$ and 20 for excitation wavelengths that corresponds to greater intensities in the PLE spectra monitored around the Eu^{3+} emission (Figure 6) (345 and 395 nm, respectively). The ϕ values change from 8.1 to 0.7% as the Eu^{3+} content increases from $n = 200$ to $n = 20$. We should point out that both values are smaller than that previously calculated using the same method for the undoped host, ca. 10%,[21] which readily indicates effective energy transfer between the di-urethanesil matrix and the Eu^{3+} cations.[16g,38] The efficiency of this energy transfer increases from 19 to 93% as the cation concentration increases. This dependence, already observed for analogous Eu^{3+}-based di-ureasils,[16g] is attributed to the fact that as the Eu^{3+} content increases more cations are located near the hybrid host emitting centers and thus enabling more efficient energy transfer. A similar observation was recently reported for a series of Eu^{3+}- and Nd^{3+}-based di-ureasil hybrids.[16g,39]

Eu^{3+} Local Coordination. Figure 9 shows in detail the RT Eu^{3+} emission lines for three selected d-Ut-(300)$_n$Eu(CF_3SO_3)$_3$ samples ($n = 200$, 10, and 5) excited under the excitation wavelength that maximizes the PL intensity, i.e., 395 nm. The spectra were displaced relative to the *y*-axis to obtain a clear view of the data. The comparison of the PL features of the three hybrids

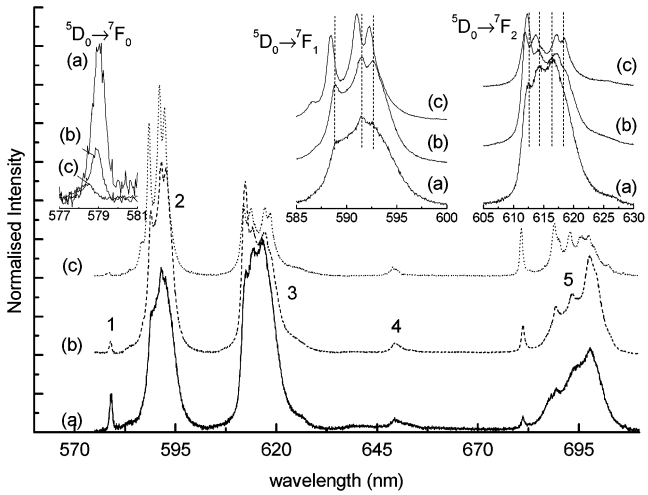

Figure 9. RT Eu^{3+} emission of the d-Ut(300)$_n$Eu(CF_3SO_3)$_3$ di-urethanesils: (a) $n = 200$, (b) $n = 10$, and (c) $n = 5$, excited under 395 nm. (1), (2), (3), (4), and (5) denote the intra-4f ^{6} transitions $^5D_0 \rightarrow {}^7F_{0-4}$, respectively.

leads us to the conclusion that changes in the energy, maximum splitting, fwhm, and number of components, in particular for the $^5D_0 \rightarrow {}^7F_{0-2,4}$ transitions, result as the Eu^{3+} content increases from $n = 200$ to 5. Changing the excitation wavelength to 345 nm, i.e., exciting the Eu^{3+} levels via the LMCT states (see Figure 6), leads to a decrease in the relative intensity of the $^5D_0 \rightarrow {}^7F_1$ transition with respect to the remaining ones. As Figure 10 confirms, the intensity of the $^5D_0 \rightarrow {}^7F_1$ transition is favored under direct excitation into the intra-4f ^{6} levels ($^5L_6$). This dependence with the excitation wavelength in the PL spectra of the three samples suggests that more than one Eu^{3+}-local coordination site might exist. To further investigate this point, the Eu^{3+} PL were measured at 10 K for the most dilute hybrid ($n = 200$). For an excitation wavelength of 345 nm, the $^5D_0 \rightarrow {}^7F_{0-2}$ transitions are composed of 1, 3, and 5 components, indicating that the Eu^{3+} ions lie in a low-symmetry local environment without inversion center (site A), according to the higher intensity of the $^5D_0 \rightarrow {}^7F_2$ transition (Figure 11). However, for 395 nm, three new Stark components are clearly discerned in the $^5D_0 \rightarrow {}^7F_1$ transition (marked with arrows in Figure 11). Taking into account that there are no differences relative to the spectrum excited at 345 nm in the $^5D_0 \rightarrow {}^7F_{0,2}$ transitions, we may infer that the second Eu^{3+} local coordination environment (site B) involves a low symmetry site with an inversion center and without $^5D_0 \rightarrow {}^7F_0$ transition.

The presence of these two Eu^{3+}-local coordination sites was further confirmed by measuring the $^5D_0$ lifetime monitored within the $^5D_0 \rightarrow {}^7F_{1,2}$ transitions under two different excitation wavelengths (345 and 395 nm). The experimental data obtained monitoring the main $^5D_0 \rightarrow {}^7F_2$ line could be fitted by a single-exponential function, revealing lifetime values of 0.27 $\pm$ 0.01 ms and 0.20 $\pm$ 0.01 ms, respectively, for 345 and 395 nm. However, the $^5D_0$ decay curve detected in the main $^5D_0 \rightarrow {}^7F_1$ line for 395 nm shows a two-exponential behavior indicating the presence of two different decay times: (i) a shorter lifetime with the same value, within the respective error, found for the decay time monitored within the $^5D_0 \rightarrow {}^7F_2$ lines, readily associated with Eu^{3+}

(38) Reinsfield, R.; Jørgenson, C. K. In *Handbook on the Physics and Chemistry of Rare Earth*; Gschneider, K. A., Eyring L., Jr., Eds.; Elsevier Science Publishers: Amsterdam, 1987; Vol. 9, p 61.

(39) Sá Ferreira, R. A.; Carlos, L. D.; de Zea Bermudez, V.; Molina, C.; Dahmouche, K.; Messaddeq, Y.; Ribeiro, S. J. L. *J. Sol-Gel Sci. Technol.* **2003**, *26*, 315.

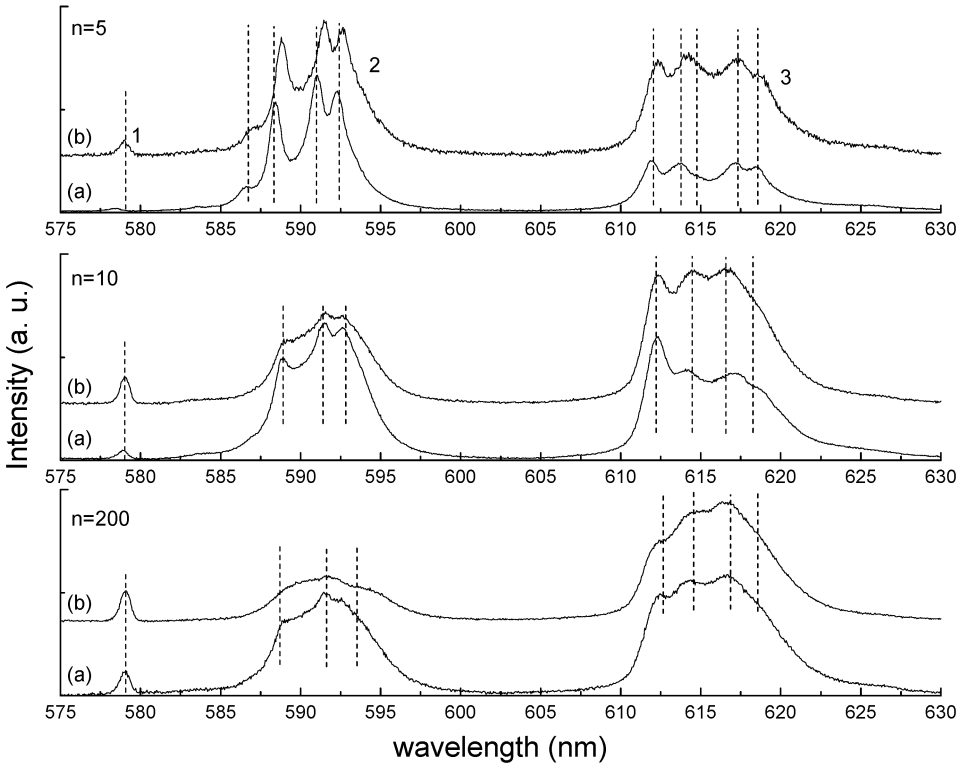

Figure 10. RT PL spectra of the d-Ut(300)$_n$Eu$(CF_3SO_3)_3$ di-urethanesils with $n = 5$, 10, and 200, excited under (a) 395 nm and (b) 345 nm. (1), (2), and (3) denote the intra-4f^6 transitions $^5D_0 \rightarrow {}^7F_{0-2}$, respectively.

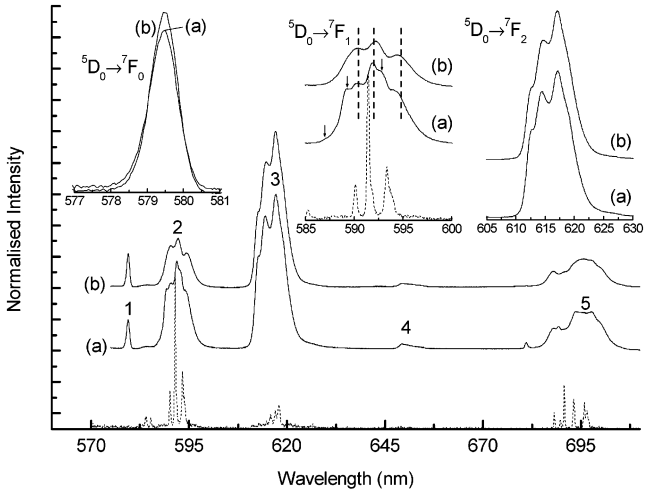

Figure 11. Low-temperature PL spectra of the d-Ut(300)-200Eu$(CF_3SO_3)_3$ di-urethanesil excited under (a) 395 nm and (b) 345 nm. The dashed line corresponds to the PL spectrum (10 K) of the Eu$(CF_3SO_3)_3$ detected under 395 nm. (1), (2), (3), (4), and (5) denote the intra-4f^6 transitions $^5D_0 \rightarrow {}^7F_{0-4}$, respectively.

site A, and (ii) a longer lifetime value, 1.40 ± 0.02 ms, ascribed to site B.

The low-temperature PL spectrum of the Eu$(CF_3SO_3)_3$ is also plotted in Figure 11. The main features of the salt emission are related with the absence of the $^5D_0 \rightarrow {}^7F_0$ transition and with the higher intensity of the $^5D_0 \rightarrow {}^7F_1$ transition. These properties are similar to those described for the Eu^{3+}-site B in the di-urethanesil host. However, comparing the energy lines and maximum split of the $^5D_0 \rightarrow {}^7F_1$ transition observed for the salt and for the hybrid, it is clear that the Eu^{3+}-site environment is not the same as that found in Eu$(CF_3SO_3)_3$. Moreover, the $^5D_0$ lifetime in the pure salt, ca. 0.1 ms,[16c] is much smaller than the value calculated for site B, reinforcing that the latter Eu^{3+} environment does not correspond to Eu$(CF_3SO_3)_3$. This conclusion is in perfect agreement with the XRD data that unequivocally demonstrate the absence of pure salt for $n > 5$.

We will now deduce the Eu^{3+} concentration dependence of the cation local environment. To monitor the number of Eu^{3+}-local coordination sites and the nature of the respective first coordination sphere, as the Eu^{3+} concentration increases, the energy and fwhm of the $^5D_0 \rightarrow {}^7F_0$ transition were estimated by deconvoluting its spectrum, assuming a Gaussian function. The analysis of the energy and fwhm of the $^5D_0 \rightarrow {}^7F_0$ transition is quite important because this transition is a nondegenerated one and its energy is usually correlated with the sum of the nephelauxetic effects arising from the Eu^{3+} first neighbors[16b,c,f−h,40,41]

For 395-nm excitation wavelength, the values found for the energy and fwhm of the site A related $^5D_0 \rightarrow {}^7F_0$ for the d-Ut(300)$_{200}$Eu$(CF_3SO_3)_3$ composite, are 17270.6 ± 0.2 cm^{-1} and 19.8 ± 0.4 cm^{-1}, respectively, as indicated in Table 3. In the case of the di-urethanesil with $n = 10$, the $^5D_0 \rightarrow {}^7F_0$ transition is also composed of one line presenting, approximately, the same energy and fwhm measured for the d-Ut(300)$_{200}$Eu$(CF_3SO_3)_3$ hybrid (see Table 3). The Stark components observed for the $^5D_0 \rightarrow {}^7F_{1,2}$ transitions are narrower, but the number and energy of the emission components is approximately the same as that previously reported for the di-urethanesil d-Ut(300)$_{200}$Eu$(CF_3SO_3)_3$. Only small changes in the relative intensity of the $^5D_0 \rightarrow {}^7F_2$ emission lines could be detected, together with an increase of the relative intensity of the $^5D_0 \rightarrow {}^7F_1$ transition. As a consequence this emission becomes the

Table 3. Energy, E (cm^{-1}), and Full Width at Half-Maximum, fwhm (cm^{-1}), of the $^5D_0 \rightarrow {}^7F_0$ Transition, Associated with Eu^{3+}-Local Coordination Sites A and C, for the d-Ut(300)$_n$Eu(CF_3SO_3)$_3$ $n = 5$, 10, and 200, Obtained under Different Excitation Wavelengths of 345 and 395 nm

	345 nm		395 nm			
	Site A		Site A		Site C	
	E	fwhm	E	fwhm	E	fwhm
$n = 200$	17269.6 ± 0.1	19.4 ± 0.2	17270.6 ± 0.2	19.8 ± 0.4		
$n = 10$	17270.5 ± 0.1	17.8 ± 0.2	17274.4 ± 0.4	18.5 ± 0.5		
$n = 5$	17271.1 ± 0.3	19.5 ± 0.7			17290.6 ± 0.4	22.5 ± 1.0

most intense line of the spectrum. The results presented suggest the presence of Eu^{3+} site A and B within the $200 \geq n \geq 10$ composition range. As Figure 9 shows, for 395-nm excitation wavelength, the further increase of the Eu^{3+} content ($n = 5$) results in an increase in the relative intensity of the $^5D_0 \rightarrow {}^7F_1$ transition, an indication that the Eu^{3+}-site B is also present in this sample. In addition, one line for the $^5D_0 \rightarrow {}^7F_0$ transition, whose energy and fwhm (17290.6 ± 0.4 cm^{-1} and 22.5 ± 1.0 cm^{-1}, respectively) are higher than the values obtained with the less-concentrated samples is discerned (Table 3). The number of Stark components observed for the $^5D_0 \rightarrow {}^7F_1$ transition increased to 4 relative to that observed for di-urethanesils with $n > 5$. Furthermore, changes were also detected in the energy of the lines of the $^5D_0 \rightarrow {}^7F_1$ transition when compared to those of the less-concentrated samples. With respect to the profile and structure of the $^5D_0 \rightarrow {}^7F_2$ emission lines, changes could be found both in the number (6) and energy of the respective Stark components. These facts, in particular the higher number of Stark components for the $^5D_0 \rightarrow {}^7F_{1-2}$ transitions and the observed changes for the $^5D_0 \rightarrow {}^7F_0$ transition (specifically, the increase in fwhm and the blue-shift with respect to less-concentrated samples), suggest a structured profile for this transition and indicate the presence of a new different Eu^{3+} local coordination site (site C) for the d-Ut(300)$_5$Eu(CF_3SO_3)$_3$ hybrid. The appearance of a new different coordination sphere for the Eu^{3+} ions in the salt-rich hybrid with $n = 5$ is supported by the analysis of the Eu^{3+} emission lines under different excitation wavelengths. As Figure 10 confirms, changes are observed in the energy of the $^5D_0 \rightarrow {}^7F_{0-2}$ transition as the excitation wavelength changes from 395 to 345 nm, clearly suggesting different Eu^{3+}-local coordination sites. Figure 10 demonstrates that the energy of the $^5D_0 \rightarrow {}^7F_{0-1}$ transitions is affected by variations in the excitation wavelength. The energy of the $^5D_0 \rightarrow {}^7F_0$ transition excited under 345 nm is red-shifted with respect to the value found at 395 nm, presenting a value (17271.1 ± 0.3 cm^{-1}) similar to the energy found for this transition in the less- concentrated samples with $n > 5$ (Table 3). This result proves that one of the Eu^{3+}-local environments found in the d-Ut(300)$_5$Eu(CF_3SO_3)$_3$ is the same as that already found in the more dilute samples with $n > 5$ (site A). In addition, the fact that the $^5D_0 \rightarrow {}^7F_1$ transition is the most intense one for both excitation wavelengths may result from the presence of free Eu(CF_3SO_3)$_3$ (see XRD results) whose PL contribution is mainly associated with such transition (Figure 11). Because of the higher number of Eu^{3+}-local coordination sites that occur for $n = 5$, the PL and PLE measurements do not clearly identify such contribution.

We now feel tempted to speculate on the nature of such Eu^{3+} local coordination sites. On the basis of the blue-shift observed for the $^5D_0 \rightarrow {}^7F_0$ transition induced by the increase in the Eu^{3+} content from $n = 200$ to 5, we may suppose that the Eu^{3+}-site C that emerges at high salt concentration has a less covalent character.[40,41] Taking into account that the covalent interaction between the ether oxygen atoms belonging to the polymer chains and the Eu^{3+} ions is weaker than that established between the oxygen atoms of the urethane carbonyl groups, we tentatively propose that the Eu^{3+}-local coordination site C that appears for $n < 10$ must involve the polyether chains. The Eu^{3+}-local coordination site A, that also exists for $n \geq 10$, is presumably associated with the carbonyl groups of the urethane linkages (i.e., the so-called cross-linked separated ion pairs, as discussed in the FTIR section). The chemical nature of the first coordination sphere of the Eu^{3+} site B involves weakly coordinated $Eu^{3+}/CF_3SO_3^-$ ionic pairs. These claims are in complete agreement with the conclusions drawn from the XRD, FT-IR, and Raman spectroscopy data discussed above.

IV. Conclusions

A family of di-urethane cross-linked poly(oxyethylene)/siloxane hybrid composites (di-urethanesils, d-Ut(300)$_n$Eu(CF_3SO_3)$_3$) incorporating a wide range of Eu(CF_3SO_3)$_3$ concentration ($\infty > n \geq 1$, where n is the molar ratio of oxyethylene moieties per Eu^{3+} ion) were prepared as transparent monoliths by the sol−gel process. Samples with $n > 5$ were found to be totally amorphous, whereas the formation of free salt occurs at higher salt content. The FT-IR and FT-Raman studies indicated that in all the xerogels examined the Eu^{3+} ions coordinate to the carbonyl oxygen atoms of the urethane cross-links and bond weakly to the $CF_3SO_3^-$ ions. In addition "free" anions were detected in the whole range of salt concentration. At $n \leq 10$ (or at a slightly lower salt concentration) the cations also interact with the ether oxygen atoms of the polymer chains of d-Ut(300). Ionic aggregates are formed in samples with $n = 5$ and 1. These results are consistent with the number of Eu^{3+} local coordination sites detected by photoluminescence spectroscopy. The Eu^{3+}-based di-urethanesil nanohybrids are promising full-color emitters with emission quantum yield ranges from 0.7 to 8.1%. The overall emission features are primarily governed by the tuning of the energy-transfer process that takes place between the hybrid's emitting centers (the NH groups of the urethane cross-links and the siloxane nanoregions) and the Eu^{3+} ions. Fine-tuning of the emission characteristics is easily achieved through

(40) Frey, S. T.; De Horrocks, W., Jr. *Inorg. Chim. Acta* **1995**, *229*, 383.
(41) Malta, O. L.; Batista, H. J.; Carlos, L. D. *Chem. Phys*, **2002**, *282*, 21.

adjustment of the lanthanide salt concentration and through the variation of the excitation energy. This outstanding feature of the d-Ut$(300)_{10}$Eu$(CF_3SO_3)_3$ xerogels widens their scope of application to include the domain of silicon-compatible display technologies requiring a fine control of an efficient white-light emission. Further studies of the effect of the molecular weight of the polyether segments of di-urethanesil-type framework on the tuning ability of the resulting Eu^{3+}-doped xerogels are clearly worth pursuing.

Acknowledgment. We thank the referees for their important suggestions and even corrections for some misinterpretations in our results appearing in the original submitted version. This work was supported by Fundação para a Ciência e Tecnologia (POCTI/P/CTM/33653/00 and POCTI/P/CTM/46780/02). D.O. thanks the National Research Council (Sweden) for financial support.

Note Added after ASAP Posting. This article was released ASAP on June 2, 2004 with a minor error in one of the references. The corrected version was posted June 8, 2004.

CM0348848